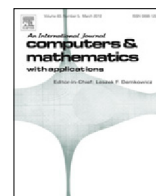




Contents lists available at ScienceDirect

## Computers and Mathematics with Applications

journal homepage: [www.elsevier.com/locate/camwa](http://www.elsevier.com/locate/camwa)

# A goal-oriented reduced-order modeling approach for nonlinear systems



Jeff Borggaard<sup>a</sup>, Zhu Wang<sup>b,\*</sup>, Lizette Zietsman<sup>a</sup>

<sup>a</sup> Department of Mathematics, Virginia Tech, Blacksburg, VA 24061, United States

<sup>b</sup> Department of Mathematics, University of South Carolina, Columbia, SC 29208, United States

## ARTICLE INFO

### Article history:

Available online 10 March 2016

### Keywords:

Reduced-order model  
Goal-oriented  
Proper orthogonal decomposition  
Burgers equation  
State estimator  
Feedback control

## ABSTRACT

In this paper, we develop a novel, goal-oriented reduced-order modeling methodology. The approach uses a low-dimensional basis function set that contains both global and local, goal-oriented basis functions. Compared to reduced-order models using the standard proper orthogonal decomposition (POD) basis, these new goal-oriented POD basis functions lead to better approximations of given quantities of interest (QoI) while maintaining accuracy in the evolution of the state. We demonstrate this approach for two problems involving Burgers equation. In the first problem, the QoI is the spatial average of the solution over various regions. The QoI in the second problem is the feedback control based on a MinMax control design with an extended Kalman filter. In both cases, approximations of the QoI and the state variables are more accurate using the goal-orientated POD than using the standard POD basis with comparable online computational costs.

© 2016 Elsevier Ltd. All rights reserved.

## 1. Introduction

Repeated numerical simulations of large-scale, nonlinear dynamical systems are required in many engineering control and optimization problems. In addition, control laws based on compensators require the real-time simulation of nonlinear models that incorporate state measurements. Direct, full-order numerical simulations require large discretized systems for adequate approximation and are not feasible in many of these applications. Thus, reduced-order models (ROMs) based on the proper orthogonal decomposition (POD) combined with Galerkin projection [1] have been widely used to provide fast, accurate simulations of these large nonlinear systems.

Essentially, POD basis functions are solution-adapted basis functions that provide the *optimal* basis to represent a given set of simulation data or snapshots. In many cases, a handful of the leading POD modes can represent the most significant characteristics of the dynamical system, e.g., patterns in turbulent flows dominated by organized (coherent) structures. However, for highly non-stationary, nonlinear problems, POD–Galerkin models may lose their effectiveness. First of all, like the Fourier basis, POD modes are global; thus energy associated with each mode is distributed throughout the domain. As a result, one may have to use a large number of POD basis functions to accurately capture the energy transfer between modes, leading to increased computational cost. Secondly, the discarded POD modes can have a marked impact on the system, see [2]. Although they only hold a fractional share of the energy, their contribution to the dynamics of the retained modes can be significant. Therefore, the POD-ROM of complex systems can be unstable even when the POD basis retained in the ROM retains 99% of energy [3]. To obtain an accurate POD-ROM for complex systems, research has been done in two main

\* Corresponding author.

E-mail address: [wangzhu@math.sc.edu](mailto:wangzhu@math.sc.edu) (Z. Wang).

directions: (i) strategies to construct a more representative basis; (ii) modeling the effects of the discarded POD modes in the ROM. In this paper, we mainly focus on the first direction. Several methods have been proposed in the literature in this direction. They aim at improving the POD basis functions: (i) by the choice of locations of snapshots [4]; (ii) by the adjustment of weights on snapshots [5–7]; (iii) by the choice of inner product [7–9]; (iv) by the enrichment of the POD basis, e.g., to minimize the residual of the ROM [10–12], to fit certain physical phenomena [13], or to account for parametric changes [14]; and (v) by the choice of the time windows on which the POD method is performed [15,16]; etc.

In this paper, we develop a new basis selection strategy for the POD-ROM to overcome the degraded efficiency when applied to complex systems. The new approach is motivated by the following key observations: The POD basis is obtained by minimizing the time average projection error of the snapshots to the space spanned by the basis on the whole spatial domain in the entire time range. Therefore the leading POD basis functions represent the global features of the system well. This basis could fail to approximate the quantity of interest (e.g., the average value of a state variable in a particular subdomain) well and fails to display the features with small time scales (e.g. the high-frequency modes in fast transient flows). Therefore, to achieve an accurate representation of the system information, the ROM basis in the proposed approach consists of *global and local* modes. The global modes are the leading POD basis functions, while, the local modes are selected for subintervals of time in a goal-oriented way.

This novel method for local mode generation synthesizes ideas from the PID method in [15] and the goal-oriented approach proposed in [5]. By considering residuals of the discrepancies between the snapshots and their projection onto the subspace spanned by global modes, we seek local modes that maximize the contribution of the residuals to the quantities of interest over short (time) subintervals. Hence, they are able to capture important small temporal scales and, usually, small spatial scales that are missed in the standard POD approximation. This new basis selection strategy leads to new physical insights into the reduced-order basis and yields an efficient, reliable way to achieve ROMs for complex systems.

The remainder of the paper is organized as follows: the POD method is briefly introduced in Section 2; the new goal-oriented model reduction method is developed in Section 3; the optimization problem is discussed in Section 4; numerical examples illustrating the effectiveness of the proposed method are presented in Sections 5 and 6. Finally, we provide brief conclusions and directions of future work.

## 2. POD-Galerkin reduced-order models

The POD-Galerkin method to produce reduced-order models for nonlinear PDEs has two main steps, computation of the POD basis and construction of the low-dimensional dynamic model through Galerkin projection. In the first step, one precomputes simulation data that is representative of the behavior expected for the surrogate model. For the Burgers equation, e.g. [17], the data consists of  $m$  finite element solutions at uniform timesteps, referred to as simulation snapshots. The POD method seeks a low-dimensional basis that optimally approximates the snapshot data. Mathematically speaking, given rank  $d$  snapshot data from a Hilbert space  $\mathcal{H}$ , it chooses  $\{\phi_1(x), \dots, \phi_r(x)\} \subset \mathcal{H}$ , for any  $r \leq d$ , to minimize the averaged projection error

$$\frac{1}{m} \sum_{\ell=1}^m \left\| w(\cdot, t_\ell) - \sum_{j=1}^r (w(\cdot, t_\ell), \phi_j(\cdot))_{\mathcal{L}_2} \phi_j(\cdot) \right\|_{\mathcal{H}}^2 \quad (2.1)$$

subject to the conditions  $(\phi_i, \phi_j)_{\mathcal{H}} = \delta_{ij}$ ,  $1 \leq i, j \leq r$ , where  $\delta_{ij}$  is the Kronecker delta. Note that other inner product spaces can be readily implemented, but  $\mathcal{H} = \mathcal{L}_2$  is typically used in practice. To solve (2.1), consider the following eigenvalue problem:

$$K \psi = \lambda \psi, \quad \text{where } K_{ij} = \frac{1}{m} (w(\cdot, t_i), w(\cdot, t_j))_{\mathcal{H}} \quad (2.2)$$

for  $1 \leq i, j \leq m$ . The so-called temporal autocorrelation matrix  $K \in \mathbb{R}^{m \times m}$  is symmetric, positive semi-definite with eigenvalues  $\lambda_1 \geq \lambda_2 \geq \dots \geq \lambda_d > 0$ , and corresponding (orthonormal) eigenvectors  $\{\psi_j\}_{j=1}^d$ . It can be shown [18–20] that the solution to (2.1) is given by

$$\phi_j(\cdot) = \frac{1}{\sqrt{\lambda_j}} \sum_{\ell=1}^m (\psi_j)_\ell w(\cdot, t_\ell), \quad 1 \leq j \leq r, \quad (2.3)$$

where  $(\psi_j)_\ell$  is the  $\ell$ -th component of the eigenvector  $\psi_j$ . The POD approximation of  $w(x, t)$  is

$$w^r(x, t) \equiv \sum_{j=1}^r \phi_j(x) a_j(t), \quad (2.4)$$

where  $\{a_j(t)\}_{j=1}^r$  are time-varying POD basis coefficient functions that must be determined. In most cases,  $r$  is chosen to be significantly smaller than both  $d$  and the number of spatial degrees of freedom (DOF) used to discretize the full-order model (FOM).

The second step in the POD-Galerkin method is to develop a dynamical system for the coefficient functions  $\mathbf{a}(t) = [a_1(t), \dots, a_r(t)]^T$ . This is achieved by substituting the POD approximation (2.4) into the full order system (e.g., the weak formulation of the PDEs), applying Galerkin projection, and using the fact that the POD basis functions are orthonormal. The POD-ROM of the Burgers equation ( $w_t = \nu w_{xx} - w w_x + f$ ) has the following form [21]:

$$\dot{\mathbf{a}} = \mathbf{b} + \mathbf{A}\mathbf{a} + \mathbf{a}^T \mathbf{B}\mathbf{a}, \tag{2.5}$$

where  $\mathbf{b}_{r \times 1}$ ,  $\mathbf{A}_{r \times r}$ , and  $\mathbf{B}_{r \times r \times r}$  correspond to the constant, linear, and quadratic terms in the numerical discretization, respectively, and the initial conditions are

$$a_i(0) = (w_0(\cdot), \phi_i(\cdot))_{\mathcal{H}} \quad \text{for } i = 1, \dots, r.$$

Note that the vector, matrix, and tensor terms above can be precomputed from  $\{\phi_1(x), \dots, \phi_r(x)\}$ , ensuring fast simulations of the POD-ROM.

While POD-Galerkin ROMs are sufficient for many nonlinear problems, the standard construction above fails in many applications unless  $r$  is chosen to be unreasonably large. Therefore, current research efforts in reduced-order modeling seek better snapshot selection strategies, improved methodologies to construct basis functions, as well as alternative models for developing (2.5). In this paper, the objective is to develop POD-based strategies to construct basis functions that improve the accuracy in computing given quantities of interest (QoI).

### 3. Systematic goal-oriented reduced-order models

In many engineering applications such as complex flow control problems, one is interested in evaluating certain quantities in real-time, e.g., the average value of a state variable in a particular subdomain, or the integral of the product of the state and a functional gain. However, as seen from the definition (2.1), the POD basis minimizes the time average approximation error on the whole domain in the entire time interval. Therefore, it usually fails to best approximate the quantity of interest. In addition, it can also fail to display the features associated with small time scales, which play a marked role in complex systems (e.g., fast transient flows). Recognizing these limitations of the POD basis, we propose a goal-oriented model reduction methodology that utilizes a mixture of global and local modes. The novelty of this approach lies in a new design of local modes.

We first regard the dominant POD basis functions,  $\{\phi_1(\cdot), \dots, \phi_{r_0}(\cdot)\}$  with  $r_0 \leq d$ , as global modes. Let  $\mathcal{Q}(\cdot)$  be a quantity of interest, which is a bounded, linear functional (see Remark 3.2). The residual of the global mode approximation to the snapshots is denoted by  $\mathcal{R}$ ,

$$\mathcal{R}(\cdot, t_\ell) = w(\cdot, t_\ell) - \sum_{j=1}^{r_0} (w(\cdot, t_\ell), \phi_j(\cdot))_{\mathcal{H}} \phi_j(\cdot). \tag{3.6}$$

Assume the simulation time is partitioned into non-overlapping time intervals, i.e.  $[0, T] = \cup_k I_k$  and for each  $k$ , time instances  $t_{k+1}, \dots, t_{k+\alpha}$  are located in the time interval  $I_k$ , then the collection of local modes on  $I_k$ ,  $\{\varphi_1^k(x), \dots, \varphi_s^k(x)\}$ , solves the following optimization problem:

$$\min_{\{\varphi_1^k, \dots, \varphi_s^k\} \in \mathcal{H}} \frac{1}{\alpha} \sum_{\ell=k+1}^{k+\alpha} \left\| \mathcal{Q}(\mathcal{R}(\cdot, t_\ell)) - \mathcal{Q} \left( \sum_{j=1}^s (\mathcal{R}(\cdot, t_\ell), \varphi_j^k(\cdot))_{\mathcal{H}} \varphi_j^k(\cdot) \right) \right\|_{\mathcal{H}}^2 \tag{3.7}$$

subject to the conditions that  $(\varphi_i^k, \varphi_j^k)_{\mathcal{H}} = \delta_{ij}$  and  $(\phi_n, \varphi_j^k)_{\mathcal{H}} = 0$ , for  $1 \leq i, j \leq s$  and  $1 \leq n \leq r_0$ .

In general, the basis obtained from (3.7) is local in both time and space, and optimally approximates the residual in the quantity of interest over given short time intervals. Therefore, the dominant local modes produce an effective representation of the small scales that are discarded in the POD truncation to  $r_0$  terms. Although this new design of local modes inherits merits from the principal interval decomposition (PID) method [15] and the goal-oriented approach [5], there are some significant differences that we highlight here. First of all, this generalizes the PID in [15], since the optimization objective in the new method is oriented by the quantity of interest. It also generalizes the goal-oriented approach in [5]. The new method does not minimize the difference between the ROM trajectory and full-order model trajectory. Instead, it minimizes the difference between the residual of snapshots and its projection onto the new basis over given intervals. Thus the optimization process here does not involve calculating and integrating the ROMs, and is computationally efficient.

The number of local basis functions in each short time interval can be selected independently such that the residual of each optimization problem (3.7) is smaller than a user-defined tolerance. Once local modes are determined, we include the leading local basis functions in the reduced-order model. Our basis generation strategy is summarized in Algorithm 1. Wherein, the global modes are the standard POD basis functions, and thus represent the most significant patterns on the whole spatial domain and over the entire time interval; and the local modes are determined from (3.7), and capture the most important patterns that contribute to the quantity of interest over the time interval  $I_k = [t_{k+1}, t_{k+\alpha}]$  and potentially on a subdomain depending on the quantity of interest. Several time interval partition methods are presented in Section 4.2.

**Algorithm 1:** Novel Basis Generation Strategy

Given solution snapshots  $\{w(\cdot, t_1), \dots, w(\cdot, t_m)\}$ .

- (1) Compute (POD) global modes,  $\{\phi_1, \dots, \phi_{r_0}\}$ , by (2.2)-(2.3).
- (2) Calculate the residuals  $\{\mathcal{R}(\cdot, t_\ell)\}_{\ell=1}^m$  of the global mode approximation to the snapshots by (3.6).
- (3) Partition the simulation time into non-overlapping subintervals  $\{I_k\}_{k=1}^{N_i}$ .
- (4) Compute goal-oriented local modes,  $\{\varphi_1^k, \dots, \varphi_s^k\}$ , on each  $I_k$  by (3.7). Details are to be presented in Section 4.1.
- (5) Collect the new basis on each  $I_k$ , i.e.,  $\{\phi_1, \dots, \phi_{r_0}, \varphi_1^k, \dots, \varphi_s^k\}$ .

The use of both global modes and local modes in the ROM enables an accurate approximation of state variables as well as the key quantity. This is particularly useful when a feedback control system is considered, in which the state (or state estimate), and the control calculation are vital. Thus, using *only* the goal-oriented basis, the ROM may have a poor approximation of the state in the areas outside those subdomains essential for the quantity of interest [5].

**Remark 3.1.** Note that the reduced-order approximation in the new basis can still be written in the same form as that of the POD approximation (2.4), on the time interval  $I_k$ , i.e., for any  $r \leq d$ ,

$$w^r(\mathbf{x}, t) \equiv \sum_{j=1}^r \bar{\phi}_j(\mathbf{x}) \bar{a}_j(t), \quad t \in I_k, \tag{3.8}$$

where

$$\bar{\phi}_j = \begin{cases} \phi_j, & j \leq r_0 \\ \varphi_{j-r_0}^k, & \text{otherwise} \end{cases}$$

and  $\bar{a}_j$  is the associated time varying basis coefficient function. Therefore, in the sequel, we refer to (3.8) as the **goal-oriented POD approximation** (GO-POD), while we refer to (2.4) as the **standard POD approximation**.

With a basis set specified over each time interval, the reduced-order models (2.5) and associated projection matrices to hand-off the simulation at the end of the current subinterval to the initial conditions of the next subinterval can all be precomputed. Thus, there is negligible online computational cost differences between the two approaches.

**Remark 3.2.** The purpose of computations in most of cases is to determine (output) a relatively small number of key quantities. For example, when control of the temperature in a warehouse is considered, the average temperature in the storage area will be the QoI in the air flow simulations. In this case,  $\mathcal{Q}(w)$  can be defined to be  $\mathcal{Q}(w) = \int_{\Omega_s} w(x, t) dx$ , where  $w(x, t)$  is the temperature and  $\Omega_s$  is the portion of the warehouse where temperature must be managed. For this study, we will consider the quantity of interest,  $\mathcal{Q}(\cdot)$ , to be a bounded, linear functional [22].

**4. Optimization formulation**

4.1. Optimization problem for local modes

Consider  $\mathcal{H} = \mathcal{L}_2$  and let  $P_j$  be the projection onto the space spanned by local basis functions  $\varphi_1^k, \dots, \varphi_j^k$ , that is,

$$P_j \mathcal{R}_\ell = \sum_{i=1}^j (\mathcal{R}(\cdot, t_\ell), \varphi_i^k(\cdot)) \varphi_i^k(\cdot).$$

We reformulate the minimization problem (3.7) as a series of unconstrained optimization problems: Seek  $\varphi_j^k \in \mathcal{L}_2$ , for  $j = 1, \dots, s$ , such that

$$\varphi_j^k = \arg \min_{\varphi_j^k} \frac{1}{\alpha} \sum_{\ell=k+1}^{k+\alpha} \|\mathcal{Q}(\mathcal{R}_\ell) - \mathcal{Q}(P_j \mathcal{R}_\ell)\|^2 + \lambda_1 (1 - \|\varphi_j^k\|^2)^2 + \lambda_2 \sum_{i=1}^{j-1} |(\varphi_i^k, \varphi_j^k)|^2 + \lambda_3 \sum_{n=1}^{r_0} |(\phi_n, \varphi_j^k)|^2. \tag{4.9}$$

Since we consider each component  $(\mathcal{Q})_i(\cdot)$  to be a linear functional,  $\mathcal{Q}$  has a discrete representation as a matrix acting on the finite element coefficients. Thus, we write  $\mathcal{Q}(w(\cdot, t)) = \mathbf{C}\mathbf{W}(t)$ , where  $\mathbf{C}$  is the coefficient matrix for the QoIs and  $\mathbf{W}(t)$  is the vector of finite element coefficients at time  $t$ . Motivated by the POD method (2.3), we use the ansatz  $\varphi_j = \mathbf{R}\psi_j$  to simplify the optimization problem. In other words, we explicitly seek the minimum in (4.9) in the range of the residual snapshots for the given time interval. Upon discretizing (4.9), we have converted the problem of solving for  $\varphi_j^k$  to minimizing

the following functional for  $\psi_j$ :

$$\begin{aligned}
 J(\psi_j) = & \frac{1}{\alpha} \sum_{\ell=k+1}^{k+\alpha} \left[ R_\ell^T C^T C R_\ell - 2 \left( \sum_{q=1}^j (\psi_q^T \mathbf{R}^T M_h R_\ell) \mathbf{R} \psi_q \right)^T C^T C R_\ell \right. \\
 & \left. + \left( \sum_{q=1}^j (\psi_q^T \mathbf{R}^T M_h R_\ell) \mathbf{R} \psi_q \right)^T C^T C \left( \sum_{q=1}^j (\psi_q^T \mathbf{R}^T M_h R_\ell) \mathbf{R} \psi_q \right) \right] \\
 & + \lambda_1 (1 - \psi_j^T \mathbf{R}^T M_h \mathbf{R} \psi_j)^2 + \lambda_2 \sum_{i=1}^{j-1} (\psi_i^T \mathbf{R}^T M_h \mathbf{R} \psi_j)^2 + \lambda_3 \sum_{n=1}^{r_0} (\phi_n^T M_h \mathbf{R} \psi_j)^2, \tag{4.10}
 \end{aligned}$$

where  $M_h$  is the finite element mass matrix.

Note that the ansatz would automatically satisfy the last constraint  $(\phi_n, \varphi_j^k) = 0$ , but this term is kept for stability. Approximate satisfaction of the orthogonality conditions on  $\varphi_j$  can later be compensated by a Gram–Schmidt procedure. Thus, the simple approximation of the constrained optimization problem in (3.7) by the unconstrained optimization problem in (4.10) does not pose any serious issues and allows us to use a fast, robust optimization algorithm. The term  $(1 - \|\varphi_j^k\|^2)^2$  leads to coercivity of the functional  $J$ . Thus existence of solutions to this unconstrained optimization problem (4.9) are guaranteed by the Weierstrass extreme value theorem. However, uniqueness of the local basis is not guaranteed, even for the  $\alpha = 3, s = 2$  case, though the sequential nature of the algorithm and judicious choices for initializing the optimization problems can provide effective solutions.

#### 4.2. Partition of the time interval

One limiting factor in using the POD basis is that time averaging can smooth out information that is only expressed over small intervals of time. Obviously, the quality of local basis functions is related to the length of subintervals  $I_k$ . A shorter time window guarantees that finer time scales are accurately represented by local modes but increases the overall computational cost. To balance the accuracy and efficiency, we consider several time interval partitioning methods.

*Clustering* Let  $\mathcal{R}_\ell = \mathcal{R}(\cdot, t_\ell)$ . A natural way to partition the time domain is to seek a few *clusters* of the residual snapshot set  $\{\mathcal{R}_1, \dots, \mathcal{R}_m\}$ . Such an idea also has been used in centroidal Voronoi tessellation (CVT)-based model reduction [23].

The clustering can be achieved by the  $k$ -means method, which minimizes the sum of squares of distances between points that belong to a cluster and the mean of the cluster. Let  $\mathcal{D}$  be a data set, it finds  $V_k \subset \mathcal{D}, k = 1, \dots, K$ , that solves

$$\min \sum_{k=1}^K \sum_{\gamma \in V_k} \|\gamma - z_k\|^2, \tag{4.11}$$

where  $z_k$  is the mean of points in  $V_k$  and  $\|\cdot\|$  is the  $\mathcal{L}_2$  norm. Utilizing Lloyd’s algorithm, we can determine the clusters and the associated centers iteratively.

*Adaptive division.* An idea presented in [15] is to compute ROMs of a given size, and adaptively grow time intervals (and update the ROM) while a prescribed error tolerance is met. Once a certified POD basis is formed over that time interval, the process moves to the next time interval. While this guaranteed accuracy is an attractive feature, this is a computationally intensive process and not likely to be a feasible in large problems.

*Equally spaced partitions.* Although not optimal, it is the most efficient and has been demonstrated to be quite effective for a number of challenging nonlinear problems [24]. We consider this approach for a number of our test cases and utilize the clustering idea above for a challenging problem where intervals need to be constructed strategically.

### 5. Simulation of 1D Burgers equation

#### 5.1. Problem description

The proposed reduced-order modeling method is first tested on a standard benchmark problem—the one-dimensional (1D) Burgers equation [17]. This model is commonly used as a one-dimensional approximation of the Navier–Stokes equations (NSE). The dynamical system associated with the NSE becomes complex when the Reynolds number is large, which corresponds to a small diffusion parameter in the Burgers equation. The Burgers equation is given as

$$\begin{cases} w_t + w w_x = \nu w_{xx} + f & \text{in } \Omega \times (0, T], \\ w(x, 0) = w_0(x) & \text{in } \Omega, \\ w(x, t) = 0 & \text{on } \partial\Omega \times (0, T], \end{cases} \tag{5.12}$$

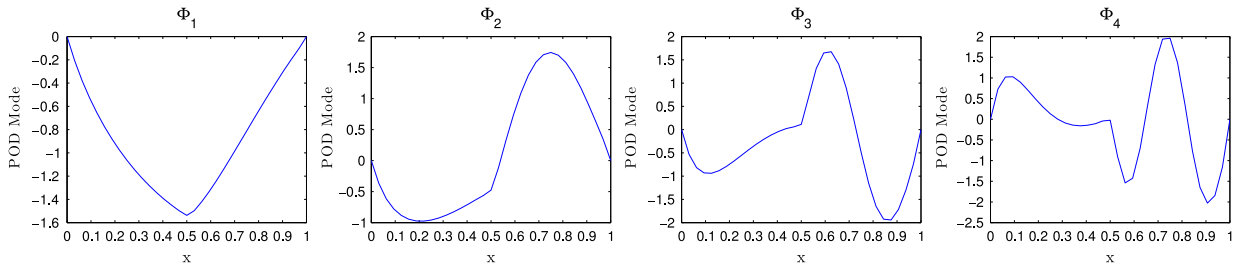


Fig. 1. First four global modes.

where  $\Omega = (0, 1)$  and  $T = 1$ . The initial condition is

$$w_0(x) = \begin{cases} 1 & \text{if } x \in \left(0, \frac{1}{2}\right] \\ 0 & \text{if } x \in \left(\frac{1}{2}, 1\right). \end{cases} \tag{5.13}$$

The finite element simulation using backward Euler for time and linear elements for space is first performed to obtain snapshots. We consider two test problems with different diffusion parameters. In particular, we consider the case  $\nu = 1 \times 10^{-2}$  from [17] and a slightly more challenging case with  $\nu = 1 \times 10^{-3}$ .

Separate studies with distinct QoI are considered. For some examples, the QoI is local (the functional  $\mathcal{Q}$  has a kernel with local support), approximating the average of  $w(\cdot, t)$  over a small region in the spatial domain, and for other examples, the QoI is global, approximating the average of  $w(\cdot, t)$  over  $\Omega$ .

5.2. Optimization problem

We use a BFGS, trust-region method [25] for the optimization problem (4.10), with the initial guess of  $\psi_j, \psi_j^0$ , satisfying  $\mathcal{R}\psi_j^0 = \frac{1}{\alpha} \sum_{\ell=k+1}^{k+\alpha} (\mathcal{R}_\ell - P_{j-1}\mathcal{R}_\ell)$ . The stopping criteria are set where either the relative step size or relative gradient are less than  $10^{-5}$ . In this unconstrained penalty formulation (4.9), we set the penalty parameters as  $\lambda_1 = \lambda_2 = \lambda_3 = 10^3$ .

5.3. Simulation study for  $\nu = 1 \times 10^{-2}$

In this study, we chose the diffusion parameter as  $\nu = 1 \times 10^{-2}$ . For the time step and mesh size, we use  $\Delta t = 1 \times 10^{-3}$  and  $\Delta x = 1/32$ , respectively. Thus a total of  $m = 1001$  snapshots are collected. One QoI averages the values of  $w$  on a small region centered at  $x = 1/32, \mathcal{Q}_1(t) = 1/3 \sum_{i=1}^3 w(x_i, t)$ , where  $0 \leq x_i \leq 1/16$ ; the other averages the values of  $w$  on a small region centered at  $x = 17/32, \mathcal{Q}_2(t) = 1/3 \sum_{i=17}^{19} w(x_i, t)$ , where  $1/2 \leq x_i \leq 9/16$ .

The first 4 POD basis functions, as shown in Fig. 1, capture over 99% of the kinetic energy of the snapshot data (the relative error in the projection is less than 0.01), and are selected as the global modes ( $r_0 = 4$ ). The time range is then divided into 10 uniform subintervals. We compute local basis functions using Algorithm 1 and the number of local basis functions,  $s$ , in each time interval is selected such that the ratio of  $|\mathcal{Q}_i(P_s \mathcal{R}_\ell)|/|\mathcal{Q}_i(\mathcal{R}_\ell)|$  is more than 0.99. It is observed that, in the process, the maximum number of local modes in each subinterval is 3. We plot the first two local modes from the first time subinterval for cases  $\mathcal{Q}_1$  and  $\mathcal{Q}_2$  in Figs. 2 and 3, respectively. It is observed that the local modes have different shapes for the different QoI.

Similar to a regular ROM, the GO-POD simulation allows the precomputation of both global and local basis functions and the ROM mass and stiffness matrices in its offline stage. For the case  $\mathcal{Q}_1$ , it takes 97.53 s to finish the offline computation. The number of iterations for finding the local basis functions on each subinterval varies from 57 to 154. Then an online stage solves the reduced-order dynamical system, which only takes about 2.18 s. In the case of  $\mathcal{Q}_2$ , the offline stage takes 114.99 s and the online stage takes 2.28 s. The iteration number in the optimization process varies from 58 to 159 in each time interval.

To verify the effectiveness of the proposed approach, we first compare solutions of (5.12) computed using the finite element method (denoted by FEM), the standard POD-ROM (denoted by POD), and our new goal-oriented approach GO-POD-ROM (denoted by GO-POD). For a fair comparison, we use  $r = 7$  POD basis functions in the standard POD-ROM since the maximum number of modes in each subinterval of the proposed approach is  $r_0 + \max(s) = 7$ . The time evolution of the finite element solution and the standard POD-ROM are shown in Fig. 4. The solutions of GO-POD-ROM for the different QoI are shown in Figs. 5 (left) and 6 (left). It is seen that the proposed approach yields better approximation than the standard POD-ROM. Indeed, the approximation error (in the  $\mathcal{L}_2$ -norm) of the standard POD is  $1.85 \times 10^{-2}$  (relative error 3.11%). Using the goal-oriented approach, the approximation errors are improved to be  $2.78 \times 10^{-3}$  (relative error 0.47%) for both  $\mathcal{Q}_1$  and  $\mathcal{Q}_2$  cases.

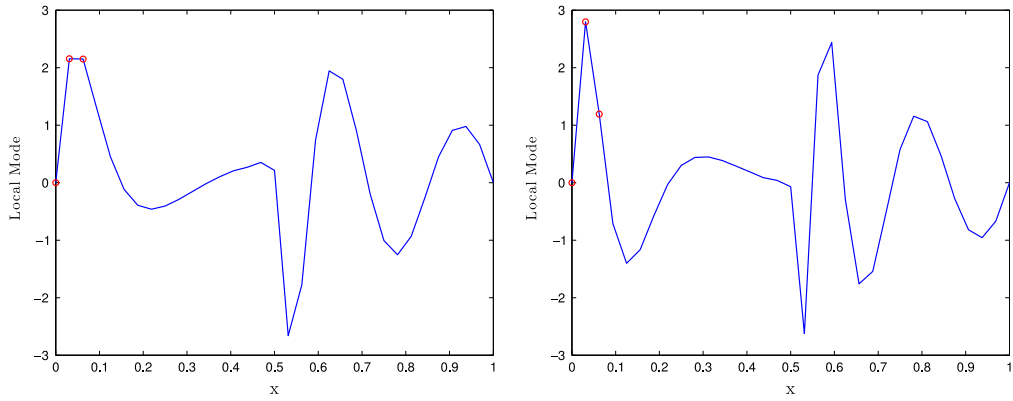


**Fig. 2.** First two local modes in the first time subinterval for  $Q_1$ : the average value of the points in red. (For interpretation of the references to color in this figure legend, the reader is referred to the web version of this article.)

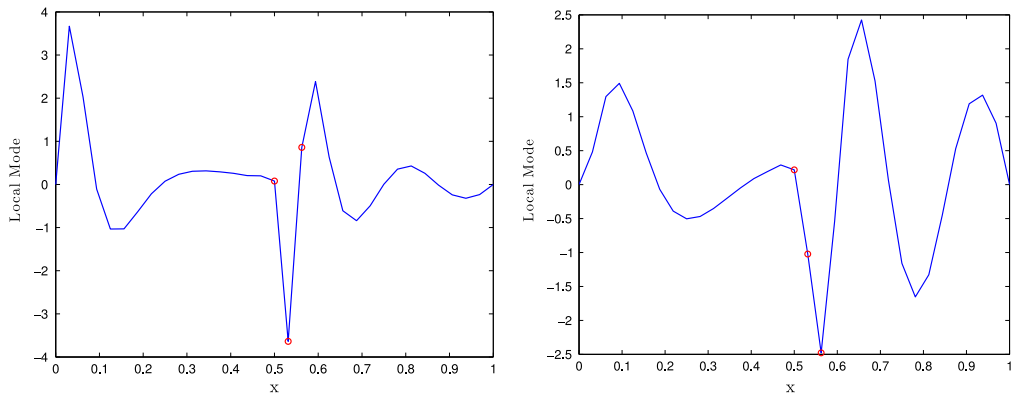


**Fig. 3.** First two local modes in the first time subinterval for  $Q_2$ : the average value of the points in red. (For interpretation of the references to color in this figure legend, the reader is referred to the web version of this article.)

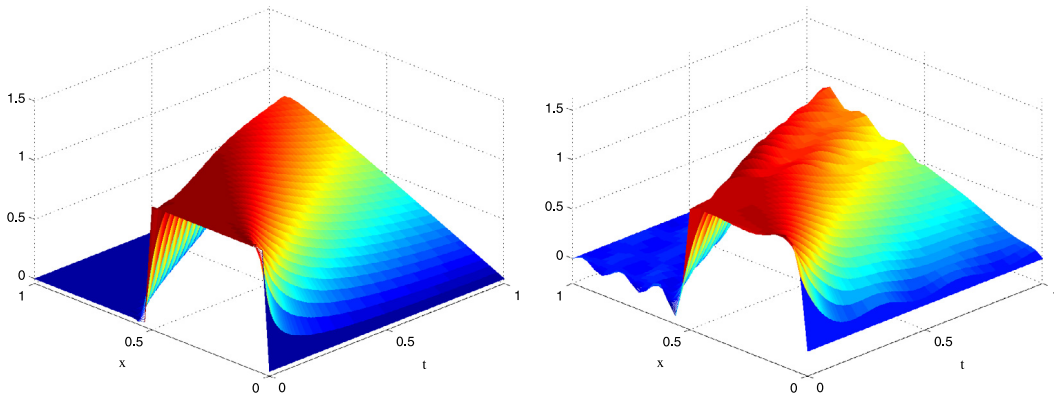


**Fig. 4.**  $\nu = 0.01$ : The finite element approximation, FEM (left) and the standard POD approximation when  $r = 7$  (right).

In the second part of the test we compare the approximation of the quantities of interest. It can be seen that the proposed approach achieves more accurate outputs than those obtained using the standard POD-ROM. As shown in Figs. 5 (right) and 6 (right), the QoI computed with the proposed GO-POD method closely track those of the FEM. In fact, the standard POD approximates  $Q_1$  with relative error 12.28% and approximates  $Q_2$  with relative error 1.84%. The new, goal-oriented approach achieves approximation of relative error 1.18% for  $Q_1$  and relative error 0.24% for  $Q_2$ .

Furthermore, we perform a sensitivity test on the penalty parameters in the optimization problem by changing  $\lambda_i = 10^5$ ,  $i = 1, 2, 3$ , the GO-POD approximation results stay the same.

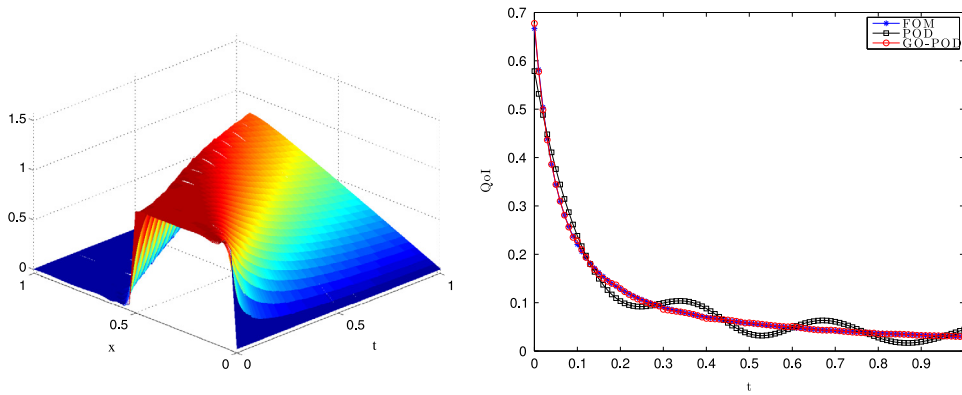


Fig. 5.  $\nu = 0.01$ : The new GO-POD approximation when  $r_0 = 4$  and  $\max(s) = 3$  (left) and the comparison of the  $Qo1, \mathcal{Q}_1(t)$  (right).

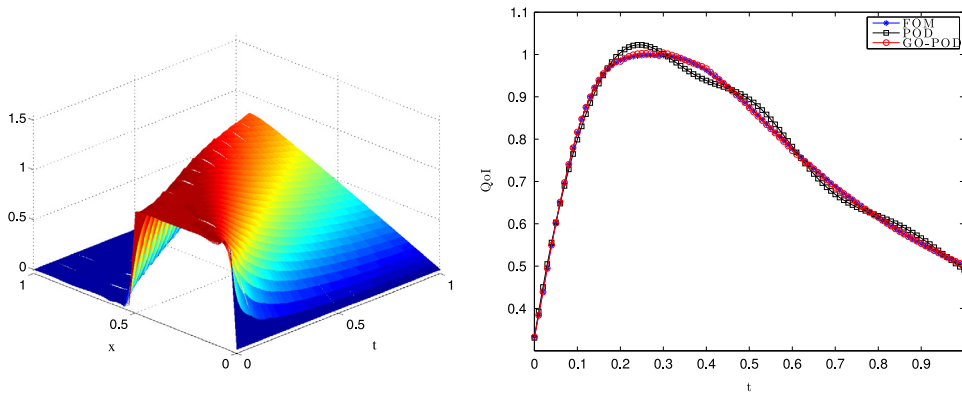


Fig. 6.  $\nu = 0.01$ : The new GO-POD approximation when  $r_0 = 4$  and  $\max(s) = 3$  (left) and the comparison of the  $Qo1, \mathcal{Q}_2(t)$  (right).

5.4. Simulation study for  $\nu = 1 \times 10^{-3}$

In this test problem, we consider 1D Burgers equation with a smaller diffusion parameter  $\nu = 1 \times 10^{-3}$ . The same time step  $\Delta t = 1 \times 10^{-3}$  but finer mesh size  $\Delta x = 1/1024$  (due to the lower viscosity) are used for the (standard Galerkin) FEM simulation. As before, a total of  $m = 1001$  snapshots are collected. Two  $Qo1$  are considered with the first being the average value of  $w$  on the whole domain,  $\mathcal{Q}_3(t) = \frac{1}{N} \sum_{i=1}^N w(x_i, t)$ . The second is the average value of  $w$  on the subdomain,  $\mathcal{Q}_4(t) = \frac{1}{N_2} \sum_{i=1}^{N_2} w(x_i, t)$ , where  $0.79 \leq x_i \leq 0.81$ .

The number of global basis functions,  $r$ , is selected such that the POD basis set  $\{\phi_1, \dots, \phi_r\}$  captures over 99% of the kinetic energy content in the snapshot set. In this test,  $r_0 = 9$  POD basis functions represent 99% of the energy and are chosen to be global modes. The time domain is then partitioned into several subintervals using the  $k$ -means clustering method on the residual snapshot set. The number of local basis functions,  $s$ , is chosen so that the ratio of  $|\mathcal{Q}(P_s R_\ell)|/|\mathcal{Q}(R_\ell)|$  is more than 0.99. Tests on the GO-POD-ROM associated with the two  $Qo1$  are implemented separately. It is observed the maximum number of local modes in every subinterval is 5. In the GO-POD-ROM simulation of case  $\mathcal{Q}_3$ , the offline stage takes 324.10 s; and the online stage takes 19.42 s to solve the reduced-order dynamical system. The number of iterations for finding the local basis functions on each subinterval varies from 90 to 261. In the case of  $\mathcal{Q}_4$ , the offline stage takes 330.75 s and the online stage takes 17.70 s. The iteration number in the optimization process varies from 62 to 272 in each time interval.

To verify the effectiveness of the proposed approach, we compare solutions of (5.12) using the finite element method (denoted by FEM), the standard POD-ROM (denoted by POD), and the GO-POD-ROM (denoted by GO-POD). To ensure a fair comparison, we keep  $r = 14$  POD basis functions in the standard POD-ROM. Fig. 7 shows the time evolution of the POD-ROM approximation solution (right) and that of the FEM solution (left). Note that the standard POD-ROM does not perform well in this case. The time evolution of the GO-POD solution associated with  $\mathcal{Q}_3$  is shown in Fig. 8 (left). The oscillations on the shock front are much smaller than that of the standard POD-ROM solution which leads one to believe that the new method has a better approximation of the state variable than the standard POD method. Indeed, the approximation error for  $w$  in the  $L_2$  norm of the standard POD is  $1.14 \times 10^{-1}$  (relative error 17.90%) while the error is improved to be  $1.26 \times 10^{-2}$  (relative error 1.98%) by using the proposed GO-POD method. The time evolution of the GO-POD approximation of  $w$  associated with  $\mathcal{Q}_4$  is shown in Fig. 9 (left). For this more challenging simulation the GO-POD-ROM also performs better than the standard

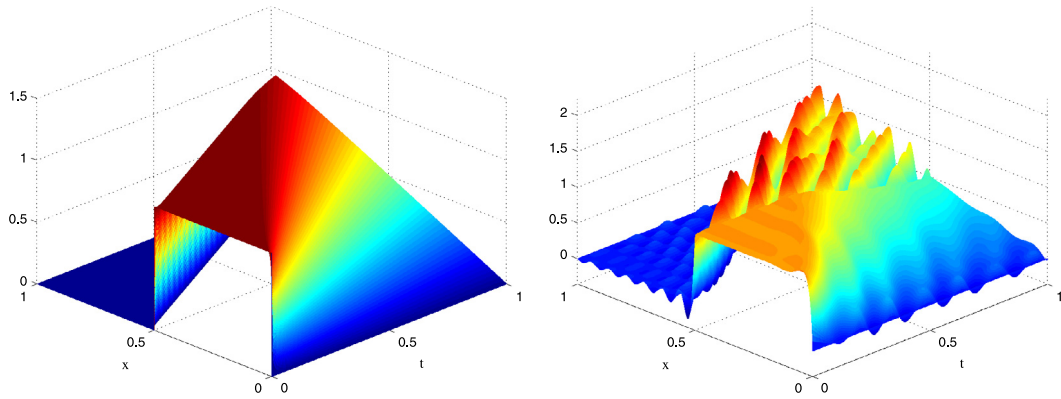


Fig. 7.  $\nu = 0.001$ : The finite element approximation, FEM (left); the standard POD approximation when  $r = 14$  (right).

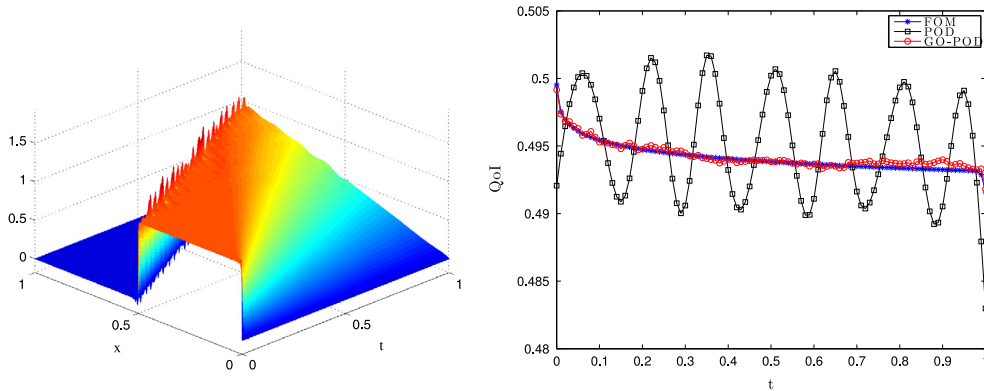


Fig. 8.  $\nu = 0.001$ : The GO-POD approximation when  $r_0 = 9$  and  $\max(s) = 5$  (left) and the comparison of the global  $QoI$ ,  $Q_3(t)$  (right).

POD method. As in the case associated with  $Q_3$ , the oscillations around the shock front are much smaller than those of the standard POD-ROM solution and the approximation error for  $w$  in the  $L_2$  norm is now reduced to  $1.34 \times 10^{-2}$  (relative error 2.11%).

Comparisons of the FEM approximation, the standard POD approximation, and the associated GO-POD approximation of  $QoI$ ,  $Q_3$ , are shown in Fig. 8 (right). The GO-POD results are close to that of the FEM solution while the standard POD approximation does not perform well. In fact, the standard POD approximation of  $Q_3$  has a relative error 0.81%, while the goal-oriented approach approximate  $Q_3$  with a smaller relative error 0.06%.

In contrast to  $Q_3$ ,  $Q_4$  is local and averages values of  $w$  on a small subdomain,  $0.79 \leq x \leq 0.81$ . Approximations of  $Q_4$  via the FEM, the standard POD approximation, and the GO-POD approximation associated with  $Q_4$  are shown in Fig. 9 (right). The relative error of the  $Q_4$  approximation is reduced to 1.97% by using the GO-POD method from the 20.77% by the standard POD method. As in the previous cases, the proposed GO-POD method provides more accurate approximations of the quantity of interest as it was designed.

## 6. Compensator-based feedback control for 1D Burgers equation

In this section, we compare reduced-order compensator-based feedback controllers using standard POD and the proposed goal-orientated POD strategies for 1D Burgers equation (5.12).

### 6.1. Control design

A MinMax control design utilizes limited state measurements to construct an estimate of the state, which is then used to define a feedback law for a control purpose. In practice, real-time control is usually desired, which motivates the reduced-order compensator-based feedback control method. We present a brief outline of the strategy in the Appendix for a nonlinear system with disturbance. For detailed discussions, the reader is referred to, e.g., [26–29] for the MinMax control design and [30,31] for reduced-order control design.

Since MinMax control theory is designed for linear systems, we will first linearize the state equation (A.3) about the zero steady state solution and design the standard linear feedback control law. The control law is obtained by adding a nonlinear

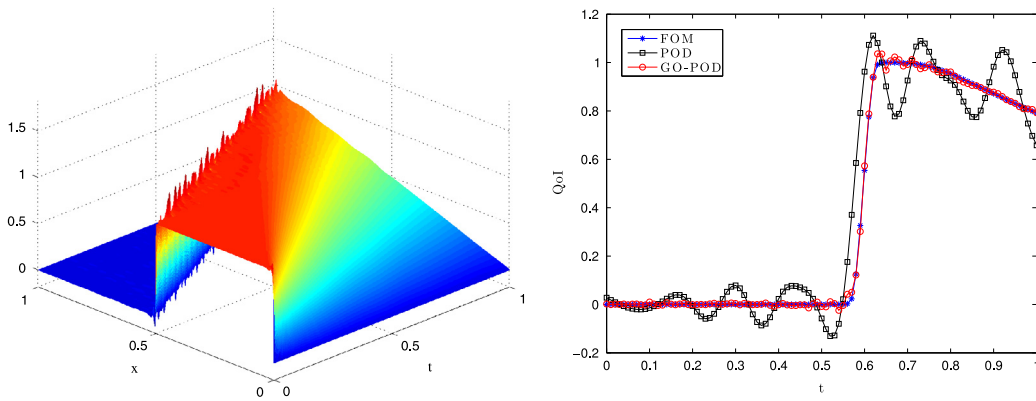


Fig. 9.  $\nu = 0.001$ : The GO-POD approximation when  $r_0 = 9$  and  $\max(s) = 5$  (left) and the comparison of the local QoI,  $Q_4(t)$  (right).

term to the linear state estimate to produce the extended Kalman filter. This nonlinearity is based on the nonlinearity in the state equation. The resulting feedback controller is nonlinear. The goal of this section is to develop a low-order controller (for fast and accurate simulations) and we compare the low-order controllers obtained using either POD or GO-POD.

6.2. Numerical test: distributed control of Burgers equation

The 1D Burgers equation with disturbance is a special case of the initial value problem (A.1), where  $Aw = \nu w_{xx}$ ,  $G(w) = -ww_x$ . We consider the problem with a diffusion coefficient  $\nu = 10^{-3}$  and Dirichlet boundary conditions  $w(t)|_{x=0} = w(t)|_{x=1} = 0$ ,  $Bu(t) = u(t, x)$ ,  $D\eta(t) = 0.75 \cos(10t)1(x)$ . The output  $y$  consists of five measurements which are average values of  $w$  over the intervals  $[0, 0.1]$ ,  $[0.2, 0.3]$ ,  $[0.4, 0.5]$ ,  $[0.6, 0.7]$ , and  $[0.8, 0.9]$ . Weights in the control design are  $R = I$ ,  $H = 10^{-5}I$  and  $Q = q(x)I$  where

$$q(x) = \begin{cases} 10 & \text{if } x \in [0.7, 0.9] \\ 1 & \text{elsewhere.} \end{cases} \tag{6.14}$$

The initial condition is

$$w_0(x) = \begin{cases} \frac{1}{2} \sin(2\pi x) & \text{if } x \in \left[0, \frac{1}{2}\right] \\ 0 & \text{if } x \in \left(\frac{1}{2}, 1\right]. \end{cases} \tag{6.15}$$

Following the strategy presented in the Appendix, we apply the POD or the GO-POD approaches to (A.9), which leads to a low-order compensator. The GO-POD ROM approach yields a similar system (A.11) as that obtained by the POD approach. The only difference lies in the different basis functions that are used. As a result, the initial condition  $a_i(0) = (w_{c_0}, \phi_i)$  for POD, but  $a_i(0) = (w_{c_0}, \tilde{\phi}_i)$  for GO-POD. For terms in the closed-loop system, for example, the  $i$ th column of  $K^r$  is  $K$  applied to  $\phi_i$  for POD, but is  $K$  applied to  $\tilde{\phi}_i$  for GO-POD; the  $i$ th row of  $F^r$  is the  $\mathcal{L}_2$  inner product of  $\phi_i$  with  $F$  for POD, but the  $\mathcal{L}_2$  inner product of  $\tilde{\phi}_i$  with  $F$  for GO-POD, etc. Next, we compare the performances of these two controllers.

For the full-order simulation we choose a mesh size  $\Delta x = 1/64$  and time step  $\Delta t = 10^{-3}$ . The open-loop (uncontrolled) simulation, and the closed-loop state and state estimate, (A.8) with  $\theta = 0$  are shown in Fig. 10. The results for the MinMax controller with  $0 < \theta \leq \theta_{\max}$  differed very little from the results using the LQG control  $\theta = 0$ . We will therefore only present the results for  $\theta = 0$ .

We first use the standard POD basis with  $r = 4$  in the reduced-order controller approximation, the simulation of the state variable and state estimation are shown in Fig. 11. The closed-loop state approximation error is  $1.01 \times 10^{-3}$  (relative error 22.01%) while just  $2.09 \times 10^{-4}$  (relative error 1.20%) for state estimate, and  $2.02 \times 10^{-4}$  (relative error 0.49%) for control variable. We then test the GO-POD method using  $r_0 = 2$  global and  $s = 2$  local modes on ten equally spaced time subintervals, the state variable and state estimation results are shown in Fig. 12. Here, the approximation error for the closed-loop state is just  $7.15 \times 10^{-5}$  (relative error 1.56%) with errors of  $6.00 \times 10^{-5}$  (relative error 0.34%) for the state estimate, and  $8.54 \times 10^{-5}$  (relative error 0.21%) for the control variable. We next only use the local modes and we choose  $s = 4$  local modes on ten equally spaced time subintervals, the state variable and state estimation results are shown in Fig. 13. The associated approximation error is  $1.80 \times 10^{-5}$  (relative error 0.39%) for state variable,  $3.66 \times 10^{-5}$  (relative error 0.21%) for state estimate, and  $5.52 \times 10^{-5}$  (relative error 0.13%) for control variable.

We then increase the reduced dimension to be 8. We first use the  $r = 8$  standard POD basis in the reduced-order controller approximation, the simulation of the state variable and state estimation are shown in Fig. 14. The approximation

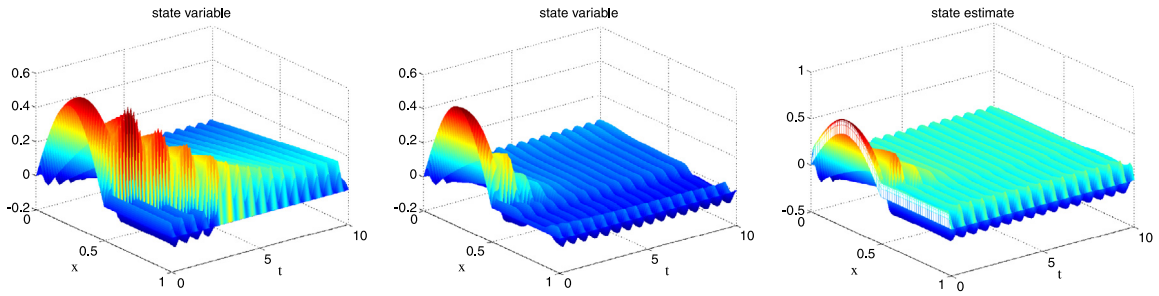


**Fig. 10.** State variable  $w(t)$  for the full-order open-loop simulation (left); Full-order closed-loop simulation with  $\theta = 0$  (middle); State estimate  $w_c(t)$  (right).

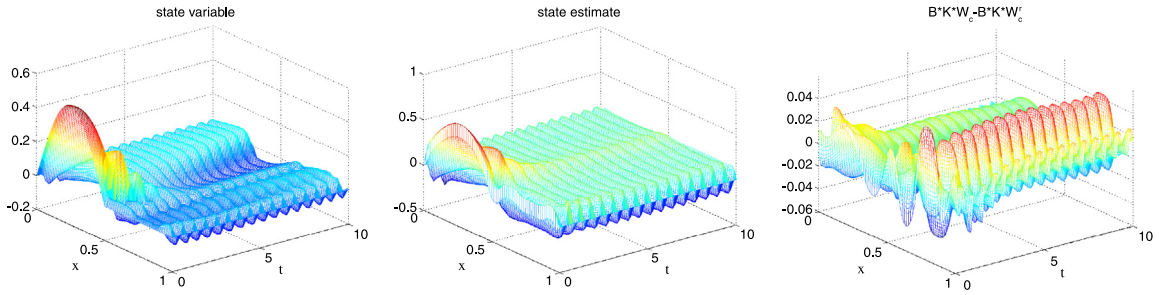


**Fig. 11.** Reduced-order LQG ( $\theta = 0$ ) feedback control system with  $r = 4$ : state variable  $w(t)$  (left), state estimate  $w_c(t)$  (center), and the control variable  $Bu(t)$  (right).

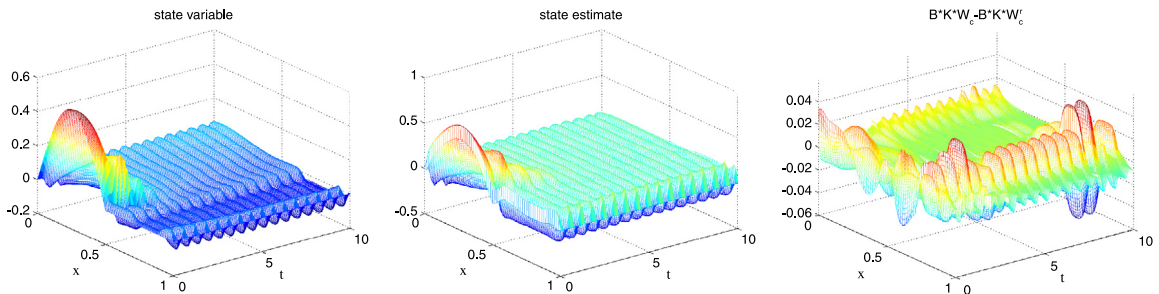


**Fig. 12.** Reduced-order LQG ( $\theta = 0$ ) feedback control system with  $r_0 = 2$  and  $s = 2$ : state variable  $w(t)$  (left), state estimate  $w_c(t)$  (center), and the control variable  $Bu(t)$  (right).

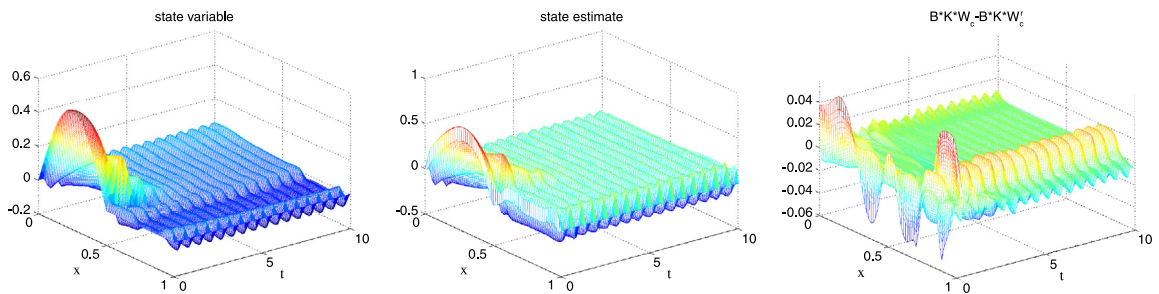


**Fig. 13.** Reduced-order LQG ( $\theta = 0$ ) feedback control system with  $s = 4$ : state variable  $w(t)$  (left), state estimate  $w_c(t)$  (center) and the control variable  $Bu(t)$  (right).

errors are  $3.85 \times 10^{-5}$  (relative error 0.84%) for the state variable,  $4.24 \times 10^{-5}$  (relative error 0.24%) for the state estimate, and  $7.33 \times 10^{-5}$  (relative error 0.17%) for control variable. We then test the GO-POD method by utilizing  $r_0 = 4$  global and  $s = 4$  local modes on ten equally spaced time subintervals, the state variable and state estimation results are shown in Fig. 15. The associated approximation errors are  $4.49 \times 10^{-5}$  (relative error 0.97%) for the state variable,  $4.03 \times 10^{-5}$  (relative error 0.23%) for the state estimate, and  $6.44 \times 10^{-5}$  (relative error 0.16%) for the control variable. Finally, we decrease the

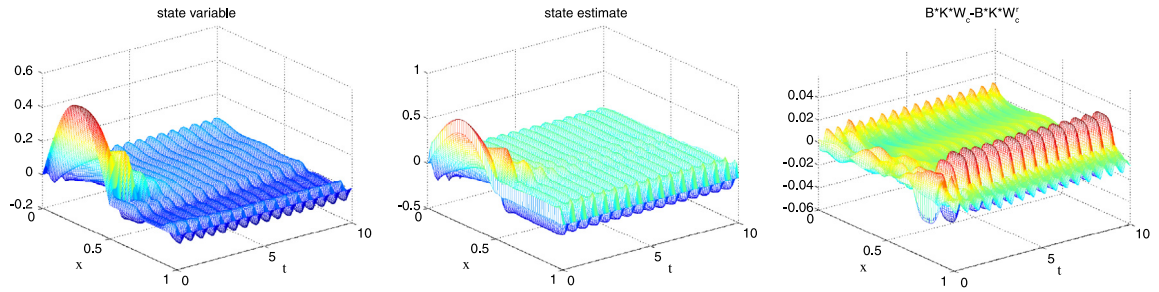


**Fig. 14.** Reduced-order LQG ( $\theta = 0$ ) feedback control system with  $r = 8$ : state variable  $w(t)$  (left), state estimation  $w_c(t)$  (middle) and the control variable  $Bu(t)$  (right).

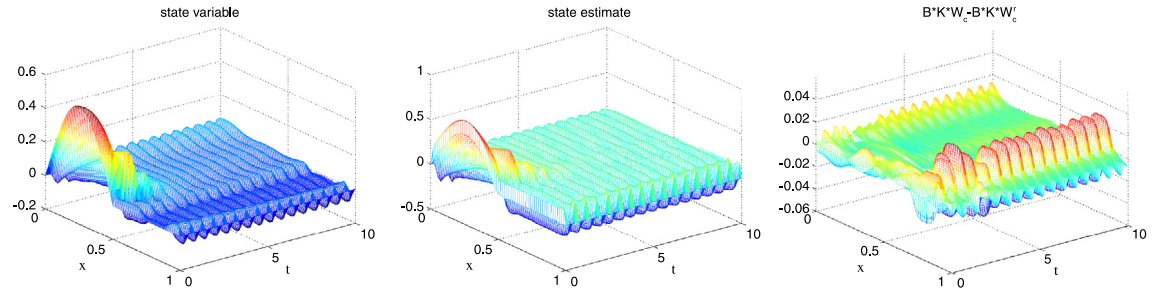


**Fig. 15.** Reduced-order LQG ( $\theta = 0$ ) feedback control system with  $r = 4$  and  $s = 4$ : state variable  $w(t)$  (left), state estimation  $w_c(t)$  (middle) and the control variable  $Bu(t)$  (right).

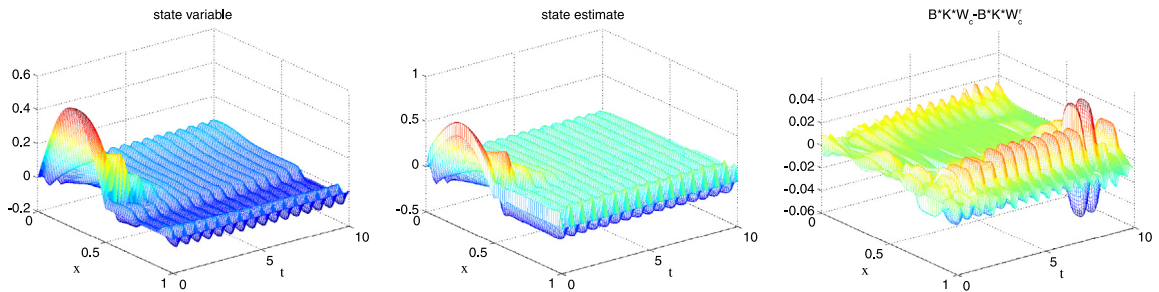


**Fig. 16.** Reduced-order LQG ( $\theta = 0$ ) feedback control system with  $r = 2$  and  $s = 6$ : state variable  $w(t)$  (left), state estimation  $w_c(t)$  (middle) and the control variable  $Bu(t)$  (right).

number of global modes again and use  $r_0 = 2$  and  $s = 6$  local modes on ten equally spaced time subintervals, the state variable and state estimation results are shown in Fig. 16. Its approximation error is  $3.49 \times 10^{-5}$  (relative error 0.76%) for state variable,  $4.18 \times 10^{-5}$  (relative error 0.24%) for state estimate, and  $5.91 \times 10^{-5}$  (relative error 0.14%) for control variable.

## 7. Conclusions and future work

We presented a goal-oriented reduced-order modeling approach that augments global POD basis functions with local goal-oriented basis functions. This approach differs from previous goal-oriented approaches in that it combines advantages of the principle interval decomposition with a more efficient optimization algorithm. The result is an effective algorithm for computing goal-oriented basis functions that are local in time. Unlike previous goal-oriented approaches, the present approach is projection based and avoids the need to build ROMs during the basis construction phase.

The GO-POD reduced-order models were demonstrated to be very effective in both simulation and compensator-based feedback-control applications. Indeed, not only were quantities of interest (QoI) computed more accurately, but the interval-based local basis functions provide better approximation properties of the dynamic nonlinear equations as well. Moreover, these advantages can be achieved with minimal additional online computational cost. The formulation of the goal-oriented basis function problem in terms of residual projection and a linear combination of snapshots significantly improves the offline computational costs as well.

There are a few natural extensions to this work. First of all, we note that possible extensions to the clustering method could be developed. For example, to distinguish the importance of some residual snapshots over others, they could be

weighted (e.g. [7]). Furthermore, snapshot residuals could be dynamically grouped to both reduce the projection error and minimize the number of ROMs that need to be built.

While the local GO-POD basis functions were local in time, they tend to emphasize structures that have local support. Finding local basis functions that capture high frequency behavior in local regions in space may have applications in complex fluid flow problems.

For the present study, we tested  $\mathcal{H} = \mathcal{L}_2$  in the construction of the global and local bases. While this proved to be very effective, alternative approaches that utilize  $\mathcal{H} = H^1$  for global bases, leading to smoother global functions, and only require  $\mathcal{H} = L_2$  for the local functions may introduce more scale separation in the bases thus providing an interesting testbed for closure modeling.

**Acknowledgments**

The authors developed the ideas for this paper while attending a workshop at the Institute for Mathematics and its Application. This research was partially supported by the Air Force Office of Scientific Research under grant FA9550-12-1-0173, the Department of Energy through the Consortium for Building Energy Innovation (CBEI), under contract DE-EE0004261, and National Science Foundation under grant DMS-1522672.

**Appendix. Reduced-order compensator-based feedback control**

Consider the following initial value problem

$$\dot{w}(t) = Aw(t) + G(w(t)) + Bu(t) + D\eta(t), \quad w(0) = w_0, \tag{A.1}$$

where  $A$  is a differential operator,  $G(\cdot)$  is a nonlinear function,  $B$  is the control input operator,  $u$  denotes the control, and  $D\eta(t)$  represents the disturbance on the system. We assume a state measurement of the form

$$y(t) = Cw(t) + E\eta(t). \tag{A.2}$$

When the MinMax control design is applied, the system is first linearized about a nominal solution. It yields the system

$$\dot{w}(t) = \tilde{A}w(t) + Bu(t) + D\eta(t), \tag{A.3}$$

where  $\tilde{A}$  contains  $A$  and the linearization of the nonlinearity  $G$  about a nominal solution. The corresponding linear state estimate,  $w_c$ , satisfies the linear equation

$$\dot{w}_c(t) = A_c w_c(t) + Fy(t), \tag{A.4}$$

and the control law is given by

$$u(t) = -Kw_c(t). \tag{A.5}$$

The operators  $K$ ,  $A_c$  and  $F$ , defined by MinMax control theory, require solutions to two algebraic Riccati equations

$$\tilde{A}^* \Pi + \Pi \tilde{A} - \Pi [BR^{-1}B^* - \theta^2 DD^*] \Pi + Q = 0, \tag{A.6}$$

$$\tilde{A}P + P\tilde{A}^* - P[C^*H^{-1}C - \theta^2 Q]P + DD^* = 0. \tag{A.7}$$

The design parameter  $\theta \geq 0$ ,  $Q$  denotes a nonnegative definite, self-adjoint state weighting operator, and  $R$  and  $H$  are positive self-adjoint weighting operators. Note that when  $\theta = 0$  the Linear Quadratic Gaussian (LQG) controller is determined.

If the nonnegative, self-adjoint solutions  $P$  and  $\Pi$  exist and  $(I - \theta^2 P \Pi)^{-1}P$  is non-negative, the operators are defined as

$$K = R^{-1}B^* \Pi,$$

$$F = (I - \theta^2 P \Pi)^{-1}P C^* H^{-1},$$

$$A_c = \tilde{A} - BK - FC + \theta^2 DD^* \Pi.$$

The largest value of  $\theta$  for which the desired solutions of (A.6) and (A.7) exist, is denoted by  $\theta_{\max}$ .

To reflect the nonlinearity in the state equation (A.1), a nonlinear state estimate equation is used

$$\dot{w}_c(t) = A_c w_c(t) + \tilde{G}(w_c(t)) + Fy(t) \tag{A.8}$$

where  $\tilde{G}$  is the difference between  $G$  and its linearization and  $\tilde{G}$  is consequently properly nonlinear in the state. Since we consider a zero steady state solution,  $\tilde{G}(\cdot) = G(\cdot)$ .

From (A.1), (A.2), (A.5), and (A.8), the resulting closed loop system can be written as the coupled system

$$\begin{bmatrix} \dot{w}(t) \\ \dot{w}_c(t) \end{bmatrix} = \begin{bmatrix} A & -BK \\ FC & A_c \end{bmatrix} \begin{bmatrix} w(t) \\ w_c(t) \end{bmatrix} + \begin{bmatrix} G(w(t)) \\ \tilde{G}(w_c(t)) \end{bmatrix} + \begin{bmatrix} D \\ FE \end{bmatrix} \eta(t) \tag{A.9}$$

with initial condition

$$\begin{bmatrix} w(0) \\ w_c(0) \end{bmatrix} = \begin{bmatrix} w_0 \\ w_{c_0} \end{bmatrix}. \quad (\text{A.10})$$

For approximation purposes we consider the finite element method for the spatial discretization. These finite dimensional discretizations of PDE systems often lead to very large systems which results in numerical challenges. For example, the high dimensional finite dimensional approximations to the operators in (A.8) require solutions to the approximations of the algebraic Riccati equations of (A.6) and (A.7). Practical implementation also requires a real-time state estimate which necessitates real-time integration of the high dimensional approximation of (A.8). A low order model for (A.1) is not the objective here since, in practice, the control will be coupled with a physical system. Instead, a low-order controller can be obtained by using the POD method.

To construct a low-order compensator one first collects a set of snapshots of the state estimate  $w_c$ ,  $\{w_c(t_0), w_c(t_1), \dots, w_c(t_m)\}$  through FEM simulation of the closed-loop system (A.9). This is computationally expensive, but is an off-line cost. Then applying one of the POD ROM approaches to (A.9) leads to a low-order compensator. The performance of this compensator can then be measured through finite element simulations of the coupled system

$$\begin{bmatrix} \dot{w}(t) \\ \dot{\mathbf{a}}(t) \end{bmatrix} = \begin{bmatrix} A & -BK^r \\ F^r C & A_c^r \end{bmatrix} \begin{bmatrix} w(t) \\ \mathbf{a}(t) \end{bmatrix} + \begin{bmatrix} G(w(t)) \\ \tilde{G}^r(\mathbf{a}(t)) \end{bmatrix} + \begin{bmatrix} D \\ F^r E \end{bmatrix} \eta(t) \quad (\text{A.11})$$

with initial condition  $w(0) = w_0$  and  $\mathbf{a}_i(0) = (w_{c_0}, \phi_i)$ , where  $\phi_i$  is the  $i$ th POD basis function. The superscripts  $r$  in (A.11) refer to new elements that arise due to operators acting on, or a Galerkin projection with a reduced-basis. For example, the  $i$ th column of  $K^r$  is simply  $K$  applied to  $\phi_i$ , the  $i$ th row of  $F^r$  is the  $\mathcal{L}_2$  inner product of  $\phi_i$  with  $F$ , etc. The important point is that in practice, one only needs to simulate

$$\dot{\mathbf{a}}(t) = A_c^r \dot{\mathbf{a}}(t) + \mathbf{a}(t)^T \mathbf{B} \mathbf{a}(t) + F^r y(t)$$

where  $y$  are given measurements. The control to the full-order system is computed as  $u(t) = -K^r \mathbf{a}(t)$ . All of the matrices and tensors in this equation can be pre-computed.

## References

- [1] P. Holmes, J.L. Lumley, G. Berkooz, *Turbulence, Coherent Structures, Dynamical Systems and Symmetry*, Cambridge University Press, Cambridge, UK, 1996.
- [2] M.J. Balajewicz, E.H. Dowell, B.R. Noack, Low-dimensional modelling of high-Reynolds-number shear flows incorporating constraints from the Navier–Stokes equation, *J. Fluid Mech.* 729 (2013) 285–308.
- [3] N. Aubry, W.Y. Lian, E.S. Titi, Preserving symmetries in the proper orthogonal decomposition, *SIAM J. Sci. Comput.* 14 (1993) 483–505.
- [4] K. Kunisch, S. Volkwein, Optimal snapshot location for computing POD basis functions, *ESAIM Math. Model. Numer. Anal.* 44 (3) (2010) 509.
- [5] T. Bui-Thanh, K. Willcox, O. Ghattas, B. van Bloemen Waanders, Goal-oriented, model-constrained optimization for reduction of large-scale systems, *J. Comput. Phys.* 224 (2) (2007) 880–896.
- [6] K. Carlberg, C. Farhat, A low-cost, goal-oriented compact proper orthogonal decomposition basis for model reduction of static systems, *Internat. J. Numer. Methods Engrg.* 86 (3) (2011) 381–402.
- [7] D.N. Daescu, I.M. Navon, A dual-weighted approach to order reduction in 4DVAR data assimilation, *Mon. Weather Rev.* 136 (3) (2008) 1026–1041.
- [8] M.F. Barone, I. Kalashnikova, D.J. Segalman, H.K. Thornquist, Stable Galerkin reduced order models for linearized compressible flow, *J. Comput. Phys.* 228 (6) (2009) 1932–1946.
- [9] A. Iollo, S. Lanteri, J.A. Désidéri, Stability properties of POD–Galerkin approximations for the compressible Navier–Stokes equations, *Theor. Comput. Fluid Dyn.* 13 (6) (2000) 377–396.
- [10] D. Amsallem, M.J. Zahr, C. Farhat, Nonlinear model order reduction based on local reduced-order bases, *Internat. J. Numer. Methods Engrg.* 92 (10) (2012) 891–916.
- [11] M. Bergmann, C.H. Bruneau, A. Iollo, Enablers for robust POD models, *J. Comput. Phys.* 228 (2) (2009) 516–538.
- [12] M. Björklund, A hierarchical POD reduction method of finite element models with application to simulated mechanical systems (Ph.D. thesis), UmeåUniversity, 2012.
- [13] B.R. Noack, K. Afanasiev, M. Morzyński, F. Thiele, A hierarchy of low-dimensional models for the transient and post-transient cylinder wake, *J. Fluid Mech.* 497 (2003) 335–363.
- [14] A. Hay, J. Borggaard, D. Pelletier, Local improvements to reduced-order models using sensitivity analysis of the proper orthogonal decomposition, *J. Fluid Mech.* 629 (2009) 41–72.
- [15] J. Borggaard, A. Hay, D. Pelletier, Interval-based reduced order models for unsteady fluid flow, *Int. J. Numer. Anal. Model.* 4 (3–4) (2007) 353–367.
- [16] W.L. Iljerman, E. van Groesen, Low-dimensional model for vortex merging in the two-dimensional temporal mixing layer, *Eur. J. Mech. B-Fluids* 20 (2001) 821–840.
- [17] K. Kunisch, S. Volkwein, Control of the Burgers equation by a reduced-order approach using proper orthogonal decomposition, *J. Optim. Theory Appl.* 102 (2) (1999) 345–371.
- [18] L. Sirovich, Turbulence and the dynamics of coherent structures. I. Coherent structures, *Quart. Appl. Math.* 45 (3) (1987) 561–571.
- [19] L. Sirovich, Turbulence and the dynamics of coherent structures. II. Symmetries and transformations, *Quart. Appl. Math.* 45 (3) (1987) 573–582.
- [20] L. Sirovich, Turbulence and the dynamics of coherent structures. III. Dynamics and scaling, *Quart. Appl. Math.* 45 (3) (1987) 583–590.
- [21] I. Akhtar, Z. Wang, J. Borggaard, T. Iliescu, A new closure strategy for proper orthogonal decomposition reduced-order models, *J. Comput. Nonlinear Dyn.* 7 (3) (2012) 034503.
- [22] M. Ainsworth, J.T. Oden, *A Posteriori Error Estimation in Finite Element Analysis*, Vol. 37, Wiley-Interscience, 2000.
- [23] J.V. Burkardt, M. Gunzburger, H.C. Lee, POD and CVT-based reduced-order modeling of Navier–Stokes flows, *Comput. Methods Appl. Mech. Engrg.* 196 (1–3) (2006) 337–355.
- [24] O. San, J. Borggaard, Principle interval decomposition framework for POD reduced-order modeling of convective Boussinesq flows, *Internat. J. Numer. Methods Fluids* 78 (2015) 37–62.
- [25] J.E. Dennis Jr., R.B. Schnabel, *Numerical Methods for Unconstrained Optimization and Nonlinear Equations*, SIAM, 1996.
- [26] T. Başar, P. Bernard, *H<sup>∞</sup> Optimal Control and Related Minimax Design Problems*, Birkhäuser, Boston, Massachusetts, 1991.

- [27] H. Marrekchi, Dynamic compensators for a nonlinear conservation law (Ph.D. thesis), Virginia Tech, 1993.
- [28] C. McMillan, R. Triggiani, MinMax game theory and algebraic Riccati equations for boundary control problems with continuous input-solution map. Part I: The general case, *Appl. Math. Optim.* 29 (1) (1994) 1–65.
- [29] I. Rhee, J.L. Speyer, A game theoretic controller and its relationship to  $H_\infty$  and linear-exponential-Gaussian synthesis, in: *Proceedings of the 28th IEEE Conference on Decision and Control*, IEEE, 1989, pp. 909–915.
- [30] J. Atwell, J. Borggaard, B. King, Reduced order controllers for Burgers' equation with a nonlinear observer, *Appl. Math. Comput. Sci.* 11 (6) (2001) 1311–1330.
- [31] J.A. Burns, B.B. King, A reduced basis approach to the design of low-order feedback controllers for nonlinear continuous systems, *J. Vib. Control* 4 (3) (1998) 297–323.